ACS APPLIED MATERIALS & INTERFACES

Research Article

www.acsami.org

Study on the Anticorrosion, Biocompatibility, and Osteoinductivity of Tantalum Decorated with Tantalum Oxide Nanotube Array Films

Na Wang,[†,‡] Hongyi Li,*[,‡] Jinshu Wang,*[,‡] Su Chen,[†] Yuanping Ma,[†] and Zhenting Zhang*[,†]

[†]Beijing Key Laboratory for Tooth Regeneration and Function Reconstruction of Oral Tissues, School of Stomatology, Capital Medical University, Tian Tan Xi Li No. 4, Beijing 100050, China

[‡]Photoelectrochemical Research Group, Key Laboratory of Advanced Functional Materials, School of Materials Science and Engineering, Beijing University of Technology, Beijing, 100124, China

Supporting Information

ABSTRACT: With its excellent anticorrosion and biocompatibility, tantalum, as a promising endosseous implant or implant coating, is attracting more and more attention. For improving physicochemical property and biocompatibility, the research of tantalum surface modification has increased. Tantalum oxide (Ta_2O_5) nanotube films can be produced on tantalum by controlling the conditions of anodization and annealing. The objective of our present study was to investigate the influence of Ta_2O_5 nanotube films on pure tantalum properties related with anticorrosion, protein adsorption, and biological function of rabbit bone mesenchymal stem cells (rBMSCs). The polarization curve was measured, the adsorption of bovine serum albumin and fibronectin to Ta_2O_5 nanotubes was detected, and the morphology and actin cytoskeletons of the rBMSCs were observed via fluorescence microscopy, and the adhesion and proliferation of the rBMSCs, as well as the osteogenic differentiation potential on tantalum specimens, were examined quantificationally by MTT and real-time PCR technology. The results showed that Ta_2O_5 nanotube films have high anticorrosion capability and can increase the protein adsorption to tantalum and promote the adhesion, proliferation, and differentiation of rBMSCs, as well as the mRNA expression of osteogenic gene such as Osterix, ALP, Collagen-I, and Osteocalcin on tantalum. This study suggests that Ta_2O_5 nanotube films can improve the anticorrosion, biocompatibility, and osteoinduction of pure tantalum, which provides the theoretical elaboration for development of tantalum endosseous implant or implant coating to a certain extent.

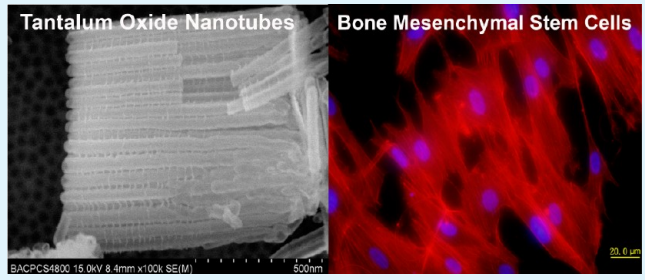

KEYWORDS: *Ta_2O_5 nanotube array, anticorrosion, protein adsorption, bone mesenchymal stem cell, osteogenesis-related genes, biocompatibility*

1. INTRODUCTION

Tantalum exhibits extreme chemical inertness at room temperature, and it is insoluble in water and acidic environments. Tantalum pentoxide has an important application as a protective coating of materials.[1] The complicated electrolyte environment within the body and various stresses on the implants easily lead to the corrosion and abrasion of endosseous implants; therefore, corrosion resistance is an important aspect regarding the survival rate of endosseous implants.[2,3] Recently, the applications of porous tantalum in artificial joints and interbody implants have demonstrated that tantalum exhibits strong bone-bonding properties.[4−6] Because tantalum has superior anticorrosion and osteoinduction, in several studies, tantalum coatings on stainless steel or titanium implants have been fabricated to enhance corrosion resistance and osseointegration.[7−11] Since it was determined that titanium dioxide (TiO_2) nanotubes array films could be produced in situ formed on titanium by anodization,[12,13] nanotubular metal oxide array films have been successively obtained on zirconium, niobium, and tantalum.[14−17] Several investigators had revealed that nanoscale topography influences cell adhesion, proliferation, and differentiation, demonstrating that nanotopography may directly influence adherent cell behavior.[18−21] In our previous studies, the microstructure of titanium dioxide (TiO_2) nanotube films improved osteoblast adhesion, proliferation, and accelerated osseointegration of early stages.[22] Popat et al.[23] also reported that tantalum nanotube arrays could enhance the proliferation and differentiation of osteoblasts. Tantalum nanotube array films were annealed under controlled conditions to obtain stable-oxide (Ta_2O_5) nanotube films, and they have greatly improved the physicochemical properties. However, hitherto, there have been no in vitro studies analyzing the biocompatibility and osteoinductivity of annealed tantalum oxide nanotube films.

In the present study, highly ordered tantalum oxide nanotube array films were produced using an anodization method. After annealing crystallization, the in vitro effects of Ta_2O_5 nanotube array films on tantalum surface properties were investigated,

Received: April 24, 2012
Accepted: August 16, 2012
Published: August 16, 2012

including anticorrosion under simulated in vivo conditions, protein adsorption, and interactions between BMSCs and nanotubes surface. The results suggest that Ta_2O_5 nanotube films can improve the biocompatibility and osteoinduction of pure tantalum. To some extent, our study offers theoretic elaboration about the development of endosseous tantalum implants.

2. MATERIALS AND METHODS

2.1. Preparation of Tantalum Oxide Nanotube Array Films. Hydrofluoric acid (HF), sulfuric acid (H_2SO_4), ethanol, and acetone were of analytical grade from Beijing Chemical Company (PRC). All compounds were used as received without further purification. Tantalum sheets (99.6% purity) were obtained from General Research Institute for Nonferrous Metals (GRINM). The tantalum sheets (10 mm × 10 mm × 0.3 mm) were cleaned in an ultrasonic bath of acetone, ethanol, and distilled water, respectively, for 10 min. The substrates were then dried in air at 80 °C. The dried tantalum sheets were anodized in 250 mL of electrolyte containing HF (5.5 mL), H_2SO_4 (223 mL), and deionized water (21.5 mL). The anodizing voltage used in this paper was 15 V, and the duration time was 90 s. The anodized samples were annealed at 500 °C for 2 h in atmosphere.

2.2. Characterization of Nanotubular Ta Oxide Films. The top morphology and alignment of the tantalum oxide nanotube films were characterized using field-emission scanning electron microscopy (FESEM; Hitachi, Model S4800) with an accelerating voltage of 15 kV. The chemical states of the tantalum surface were analyzed by X-ray photoelectron spectroscopy (XPS). The phase composition was characterized using X-ray diffraction (XRD).

2.3. Polarization Curve Measurements. High-glucose Dulbecco's Modified Eagle's Medium (DMEM) and fetal bovine serum (FBS) was purchased from Gibco Company. The polarization curve experiment was performed at room temperature in a three-electrode system, which was established on a beaker (made of quartz) containing a 500-mL test solution (DMEM containing 10% FBS). A saturated calomel electrode (SCE) and platinum electrode served as the reference electrode and the counter electrode, respectively. The pure tantalum and the anodized tantalum, used as the work electrode, were vertically immersed into the solution with 1 cm^2 exposed to the electrolyte solution. The polarization curves of pure tantalum and anodized tantalum were tested respectively. All experiments were repeated by using different specimens to confirm the reproducibility of the results.

2.4. Contact Angle Measurements. Contact angle (CA) measurements on untreated tantalum surface and the surfaces of the Ta_2O_5 nanotubes were carried out at room temperature using a commercial contact analysis system (Model OCA20, Dataphysics Co., Ltd.) by the sessile drop method. The mean value of the contact angle was calculated from at least five individual measurements taken at different locations on the examined specimens. The surface free energy of untreated tantalum and Ta_2O_5 nanotube array films were obtained by measuring the contact angle with the aid of a test fluid whose surface energy is known. In our case, three liquids (distilled water, diiodomethane, and ethylene glycol) were used as probe liquids for the acquisition of the contact angle, and the total surface energy was calculated according to the method described previously.[24]

2.5. Protein Adsorption Assay. Bovine serum albumin (BSA) and fibronectin (sigma) were used as model proteins. Two hundred microliters (200 μL) of protein solution (1 mg/mL) was pipetted onto the tantalum specimens. After incubation for 2 and 24 h at 37 °C, the specimens were transferred to a new 24-well plate (one sample per well) and washed thrice with phosphate-buffered saline (PBS, pH 7.4). Two hundred microliters (200 μL) of a 2% sodium dodecyl sulfate (SDS) solution were added to these wells and shaken for 2 h to detach proteins from the tantalum surfaces. The protein concentrations in the collected SDS solutions were determined using a MicroBCA protein assay kit (Pierce) and quantified using a microplate spectrophotometer (SPECTRA max PLUS384) at 562 nm. The total amounts of protein adsorbed on the untreated tantalum and Ta_2O_5 nanotubes surface were respectively determined using a standard curve drawn with BSA.

2.6. Mesenchymal Stem Cells Culture. Rabbit bone mesenchymal stem cells (rBMSCs) were isolated from fresh bone marrow from the femurs of three-month-old New Zealand rabbits, as described previously.[25] The experimental protocol in this study was reviewed and approved by the Animal Care and Use Committees of Capital Medical University, China. rBMSCs were cultured in high-glucose Dulbecco's Modified Eagle's Medium (DMEM) with 10% fetal bovine serum (FBS) (Gibco) and 1% penicillin/streptomycin (PS). The cells were cultured in a 5% CO_2 incubator at 37 °C. Culture media were changed every 2 or 3 days. After cell isolation and expansion, in the osteogenesis and adipogenesis differentiation media, the expanded cells showed multipotent potential to differentiate into multiple mesenchymal lineages, including osteoblasts and adipocytes (see Figure S1 in the Supporting Information).

2.7. Fluorescence Microscopy Observation of Adherent rBMSCs. rBMSCs were seeded on each tantalum specimen at a density of 1 × 10^3 cells/cm^2 and were incubated in a 5% CO_2 incubator for 1, 2, 24, and 48 h, respectively, and washed twice with prewarmed PBS (pH 7.4). The cells on the specimens were fixed with 3.7% formaldehyde for 10 min, and then treated with 1% Triton X-100. All samples were blocked with 2% BSA for 30 min, and the action cytoskeletons were labeled by incubating with Alexa Fluor 594 Phalloidia (Invitrogen) for 30 min at room temperature in darkness. After rinsing with PBS, the cell nuclei were contrast-labeled by DAPI (Invitrogen) for 5 min. The morphology of rBMSCs and actin cytoskeletons on the untreated tantalum surface and the surfaces of the Ta_2O_5 nanotubes were visualized with an inverted fluorescence microscope (Olympus, Model IX71).

2.8. rBMSCs Adhesion and Proliferation Detected with MTT Assay. rBMSCs adhesion and proliferation on untreated surfaces and the surfaces of Ta_2O_5 nanotubes were investigated with MTT assay on days 1, 2, 3, 4, 5, 6, and 7 after seeding the cells. One hundred microliters (100 μL) of cell suspension (5 × 10^4 cells/mL) were seeded onto each specimen and incubated in a 5% CO_2 incubator for 1 h, to allow cells to attach to the tantalum surfaces, and then 2 mL of medium were added in each well and further incubated for the set periods. At the selected incubation time point, the samples were washed by PBS and transferred to a new 24-well polystyrene culture plate with 1 mL of culture medium in each well; then, 100 μL of MTT (5 mg/mL, Sigma) was added to each well. After 4 h of incubation in a 5% CO_2 incubator, all culture media were removed, 750 μL of dimethylsulfoxide (DMSO) was added to each well, and the 24-well polystyrene plate was shaken for 10 min. One hundred fifty microliter (150 μL) solutions of each well were transferred to a 96-well polystyrene plate. The absorbance of solution was measured at the wavelength of 490 nm with a microplate spectrophotometer (Model SPECTRA max PLUS384).

2.9. Osteogenesis-Related Gene Expressions. *2.9.1. Cell Culture.* rBMSCs P3 were seeded on untreated surfaces and the surfaces of Ta_2O_5 nanotubes, respectively, at a cell density of 3 × 10^4 cells/cm^2 and grown in growth media. Following overnight incubation, specimens were carefully rinsed, and incubation in an osteogenesis differentiation medium (Gibco) was continued; this represented the starting time point (T = 0). The osteogenic medium was replaced every third day. Specimens with adherent cells and forming tissue layers were collected on days 3, 7, 10, and 14 for real-time PCR analysis.

2.9.2. RNA Isolation and Analysis. To evaluate the mRNA expression of cells adherent to tantalum surfaces, adherent cells on each specimen were lyzed with Trizol (Invitrogen). The total RNA in the cell lysate was isolated and collected. Total RNA was quantified using UV spectrophotometry. From each total RNA sample, reverse transcription was carried out using M-MLV RTase cDNA Synthesis Kit (TaKaRa). All cDNAs were subjected to polymerase chain reaction (PCR) for GAPDH mRNA as a test of RNA integrity and cDNA synthesis. Subsequently, equal volumes of cDNA were used to program real-time PCR reactions specific for mRNAs encoding ALP, Collagen-I (Col-I), Osterix (Osx), and Osteocalcin (OC). Design of

primers for ALP, Col-I, Osx, OC, and GAPDH was performed using the Primer3 and NCBI blast software (see Table 1).

Table 1. Primers of Target and Housekeeping Genes[a]

gene	primer sequence	amplicon size (bp)
Osterix	S: 5′CTCCAAGCGCTTCACCCGGA-3′	96
	A: 5′CTCCAAGCGCTTCACCCGGA-3′	
ALP	S:5′TTGCGCACGTCATGGCCCTC-3′	72
	A: 5′CCCCATTAGGGGGCGTCACAT-3′	
Collagen-I	S:5′ TGCGACATGGACACTGGGGC-3′	158
	A:5′ GAGCCTTCGCTGCCGTACTCG-3′	
Osteocalcin	S: 5′GGCGCCAACTGATCGACGGG-3′	86
	A:5′CGGGTTGAGCTCGCACACCT-3′	
GAPDH	S:5′TCCCGTTGCTGTCGCCCGTT-3′	113
	A:5′GCGCCCAATGCGGCCAAATC-3′	

[a]Oligonucleotide sequences of sense (S) and antisense (A) primers of target and housekeeping genes used in the real-time PCR and amplicon size (base pairs) of the resulting PCR products.

Real-time PCR was performed in duplicates using BioEasy SYBR Green I Real-Time PCR Kit (SUNBIO, China) in the Line-Gene Real-Time PCR Detection System (BIOER, Hangzhou, China), a total volume of 50 mL of PCR mixture (which included 25 mL of 2 × SYBR Mix, 1 mL of PCR Forward Primer, 1 mL of PCR Reverse Primer, 0.3 mL of Taq DNA Polymerase, 20.7 mL of double-distilled H_2O_2, and 2 mL of template cDNA) were loaded in each well of the PCR array. PCR amplification was conducted with an initial 2 min step at 95 °C, followed by 45 cycles of 95 °C for 20 s, 59 °C for 25 s, and 72 °C for 30 s. The fluorescence was read at the end of the 72 °C step. Melting curves were recorded after the run by stepwise temperature increase (0.5 °C/s) from 70 °C to 95 °C. The fluorescent signal from SYBR Green was detected immediately after the extension step of each cycle, and the cycle at which the product was first detectable was recorded as the cycle threshold. The housekeeping gene GAPDH was used as the internal control gene to normalize the quantities of target genes. Relative mRNA abundance was determined by the $2^{-\Delta\Delta Ct}$ method and reported as fold induction.

3. RESULTS AND DISCUSSION

3.1. Surface Characterization. *3.1.1. Characterization of Tantalum Oxide Nanotube Films.* Figure 1 describes the top morphology and cross section of tantalum oxide nanotube array films, which were anodized under 15 V for 90 s and annealed at 500 °C for 2 h. The highly ordered tantalum oxide nanotube arrays clearly have been formed on the surface of the tantalum substrates. Based on the morphology shown in Figure 1, the diameter and the length of the nanotubes were measured to be ∼20 nm and ∼920 nm, respectively. Figure S2 in the Supporting Information describes the phase composition of pure tantalum, as well as anodized tantalum before and after being annealed at 500 °C for 2 h (ramp = 2 °C/min). Ta_2O_5 (Figure S2c in the Supporting Information) clearly appeared after the material was annealed; however, the intensity of Ta_2O_5 is quite weak, because of the relatively short length (920 nm) of Ta_2O_5 nanotube. In addition to Ta_2O_5, γ-TaO_x is also found on anodized tantalum after annealing, because of the oxidation of the tantalum substrate, which can be verified by the formation of γ-TaO_x (see Figure S2d in the Supporting Information) on the surface of annealed pure tantalum.

3.1.2. XPS Analysis of Tantalum Oxide Nanotube Films. XPS analysis was used to determine the chemical composition and state of nanotubular tantalum oxide films on tantalum. XPS results show that the outermost layers of oxide mainly contained Ta, O, C, and S. Figure 2a shows Ta 4f peaks in pure Ta and anodized samples annealed at 500 °C for 2 h. For pure tantalum, there are two types of Ta chemical states: (1) Ta 25.7 and 27.5 eV, in the Ta_2O_5 state, and (2) Ta 20.5 and 22.3 eV, in the metallic state.[26,27] The oxygen-to-tantalum ratio was 2.59, as measured by XPS quantitative analysis. When anodized tantalum specimens annealed at 500 °C for 2 h, only one chemical state appeared, Ta 25.7 and 27.5 eV in the Ta_2O_5 state. Based on the XPS quantity analysis, the oxygen-to-tantalum ratio was 2.63, higher than that of pure tantalum. The XPS results (Figure 2a) combined with XRD analysis (Figure S2 in the Supporting Information) made us believe that a layer of Ta_2O_5 nanotube array films was formed on the surface of Ta substrate after anodization and annealing

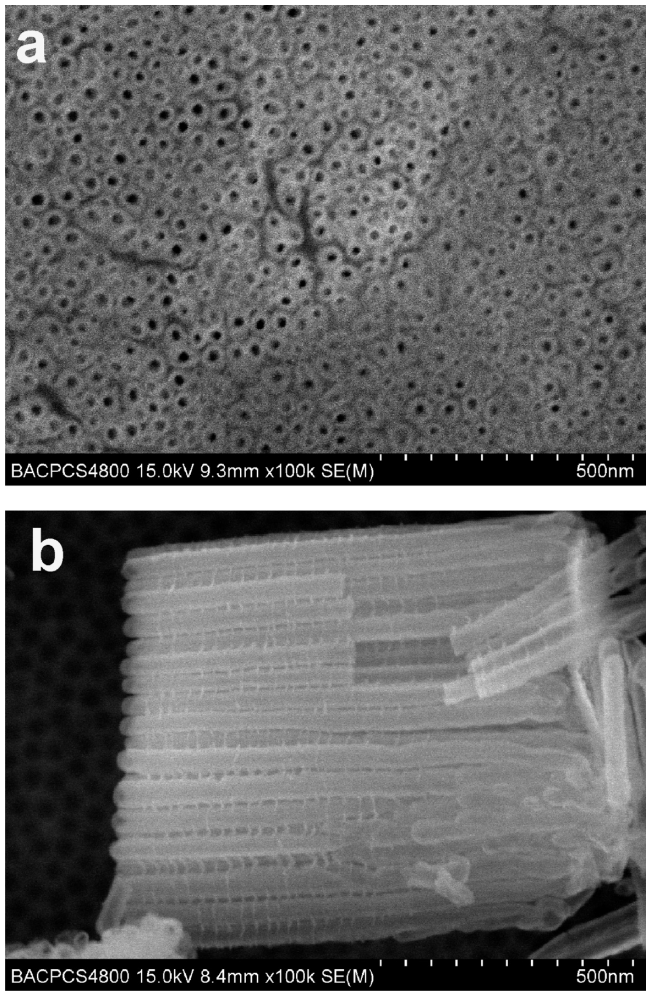

Figure 1. (a) SEM top morphology and (b) section alignment of Ta_2O_5 nanotubes fabricated using an anodization method.

3.2. Polarization Curve Measurements. Figure 2b illustrates the polarization curves of untreated tantalum and anodized tantalum annealed at 500 °C for 2 h. The corrosion potential and corrosion current density of untreated tantalum is −0.4 V (vs SCE) and $\sim 10^{-8}$ A/cm^2, respectively. Meanwhile, for the anodized tantalum sample annealed at 500 °C for 2 h, the corrosion potential is −0.328 V (vs SCE) and the corrosion current density is $\sim 10^{-9}$ A/cm^2.

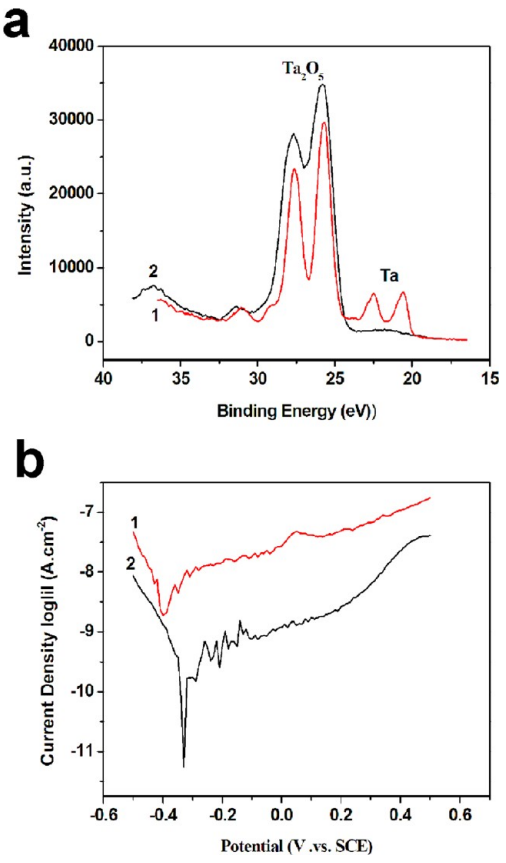

Figure 2. (a)Ta 4f X-ray photoelectron spectroscopy of (1) pure tantalum and (2) anodized tantalum annealed at 500 °C for 2 h in atmosphere. (b) Polarization curves of (1) untreated tantalum and (2) anodized tantalum annealed at 500 °C for 2 h. The test solution is DMEM containing 10% FBS at room temperature.

After anodization and annealing at 500 °C, the anticorrosion of tantalum is enhanced (Figure 2b), which attributed to Ta_2O_5 nanotube films formed on the surface of the tantalum substrate. The tantalum oxides formed on the tantalum surface provide a barrier, which prevents the release of metal ions from the metal matrix to the electrolyte. The biocompatibility of a material is closely related to the ability to remain biologically innocuous during its functional period inside a living creature, so the corrosion resistance is an important aspect about the biocompatibility for a metallic biomaterial.[2,3] In our study, through comparison to untreated tantalum surfaces, we found that the surfaces of Ta_2O_5 nanotubes have significant higher anticorrosion in DMEM containing 10% FBS, which suggests that Ta_2O_5 nanotube films possess excellent biocompatibility; therefore, implant decorated Ta_2O_5 nanotube films might hardly cause cytotoxicity, allergy, and chronic inflammation.

3.3. Contact Angle and Surface Energy. The water contact angle and total surface energy of untreated tantalum surface and modified Ta_2O_5 nanotube films are shown in Table 2. There were significant differences in both water contact angle and surface energy between the untreated tantalum and Ta_2O_5 nanotubes surface ($P < 0.01$). In biological systems, the wettability and surface energy of implant surface plays an important role in the mediation of solute adsorption and cell adhesion.[28−32] In our study, the surface modifications of Ta_2O_5 nanotube films improved the hydrophilicity and surface energy of pure tantalum, and the enhanced hydrophilicity and surface energy were consistent with improved protein adsorption and the biological function of rBMSCs on a nanotubular surface.[28,30−32]

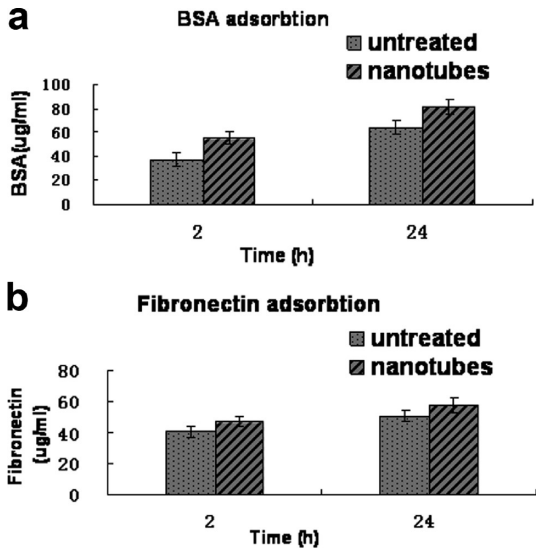

Figure 3. Protein adsorption on untreated and Ta_2O_5 nanotubes surface after incubation for 2 and 24 h. Significantly more protein is adsorbed on the surfaces of the Ta_2O_5 nanotubes than on untreated tantalum surface ($P < 0.01$) ((a) bovine serum albumin (BSA) and (b) fibronectin (Fn)).

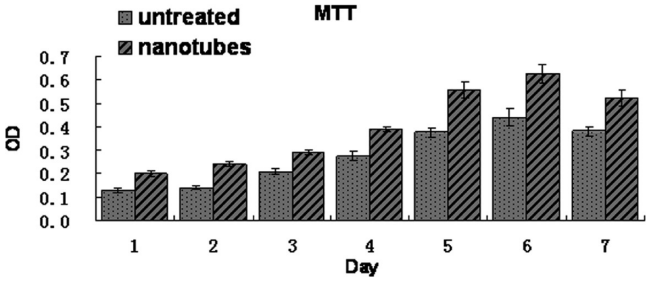

Figure 4. For adhesion and proliferation of rBMSCs at day 1, 2, 3, 4, 5, 6, and 7, the MTT assay showed that there was significant difference between the untreated tantalum surface and the surfaces of the Ta_2O_5 nanotubes at all incubation times ($P < 0.01$); the optical density (OD) value increased rapidly from day 3, and reached its highest level at day 6, and then the OD value began to drop after day 6.

3.4. Protein Adsorption. The amount of BSA and fibronectin (Fn) adsorbed on the surface after incubation for 2 and 24 h was assayed, and the results are displayed in Figure 3; significantly more protein is adsorbed on the surfaces of the

Table 2. Water Contact Angle and Total Surface Energy of Untreated Tantalum Surface and Modified Ta_2O_5 Nanotube Films

	contact angle (deg)			
sample	water	diiodomethane	ethylene glycol	surface energy (mJ/m^2)
untreated tantalum	70.5 ± 3.9	49.3 ± 4.1	53.9 ± 4.5	35.628 ± 4.27
anodized tantalum	30.5 ± 4.1	39.7 ± 2.4	7.2 ± 1.7	68.553 ± 4.18

dx.doi.org/10.1021/am300727v | ACS Appl. Mater. Interfaces 2012, 4, 4516−4523

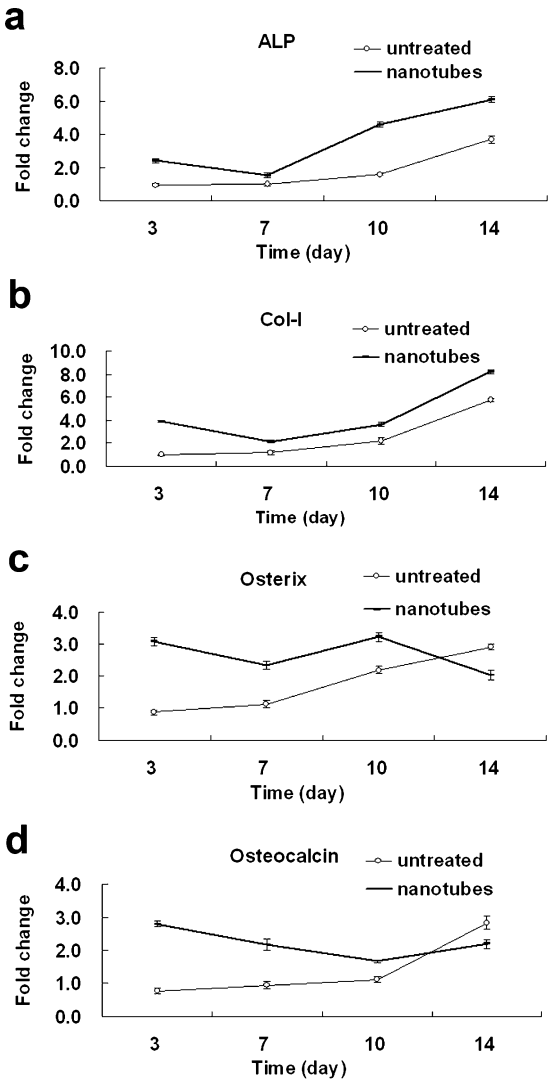

Figure 5. The mRNA expression of the osteogenesis-related genes of differentiated rBMSCs on the untreated tantalum surface and the surfaces of the Ta_2O_5 nanotubes. At (a) day 3, (b) day 7, (c) day 10, and (d) day 14, there was a significant difference on genes expression of ALP, Col-I, Osx, and OC between the untreated tantalum surface and the surfaces of the Ta_2O_5 nanotubes ($P < 0.05$).

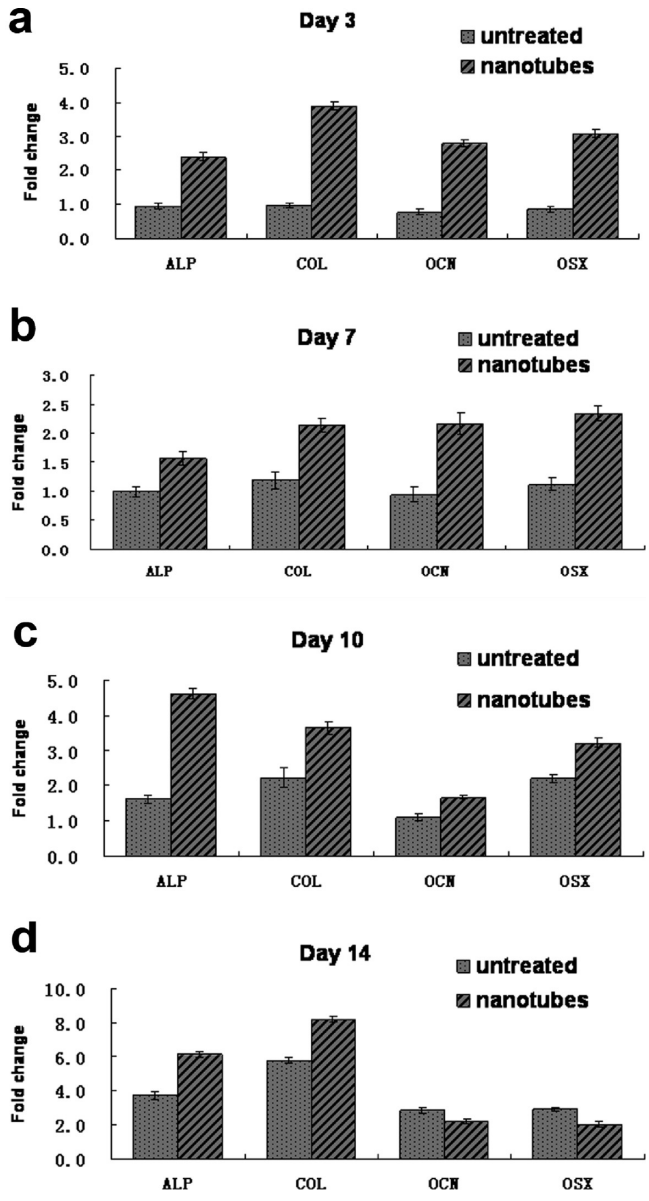

Figure 6. Osteogenesis-related mRNA expression trend on the untreated tantalum surface and the surfaces of the Ta_2O_5 nanotubes. At day 3, 7, 10, and 14, the temporal pattern of expression levels for (a) ALP, (b) Col-I, (c) OSX, and (d) OC is shown in terms of fold change.

Ta_2O_5 nanotubes than that absorbed onto the untreated surface ($P < 0.01$). The higher protein adsorption of surfaces of the Ta_2O_5 nanotubes is correlated with its nanoscale topography and hydrophilicity.[−3033] The ability of materials to adsorb proteins from serum determines their ability to support cell adhesion and spreading;[3237] hence, it is an important aspect of their biocompatibility. Serum albumin, which constitutes ∼60% of human plasma protein, serves as a carrier for molecules of low water solubility (for example, albumin-bound lipids that stimulate osteoblast proliferation).[34] For maximum concentration, and because of a faster diffusion coefficient, serum albumin will first reach and adsorb onto the implant surface, and then, it be displaced by proteins (e.g., Fn) with a higher affinity for metallic oxide surface.[35] Fn is responsible for key functions such as provision of a structural framework for cell attachment, migration, and differentiation through integrin receptors.[36,37] After implantation, along with fibrin, plasma fibronectin is deposited at the site of implantation, forming a blood clot between the implant and bone cavity, then bone mesenchymal stem cells (BMSCs) migrate to the surface of the implant and differentiate.[36,37] In this study, the Fn adsorption capacity of the surfaces of the Ta_2O_5 nanotubes is superior to that of untreated tantalum surface, which suggests that Ta_2O_5 nanotube films can enhance osteoinductivity of pure tantalum and promote osteogenesis around tantalum implants. In addition, after incubation for 2 and 24 h, the adsorbed protein on the tantalum surface is different in our study (see Figure 3). This result was in disagreement with some previous research that had indicated that an adsorption maximum is reached within an average time of 30 min,[38] which was most likely attributed to the fact that other studies used different protein concentration and testing methods, different materials, or materials with different surface properties.

3.5. MTT Assay. The adhesion and proliferation of rBMSCs cultured on different tantalum surfaces are indicated in Figure

dx.doi.org/10.1021/am300727v | ACS Appl. Mater. Interfaces 2012, 4, 4516−4523

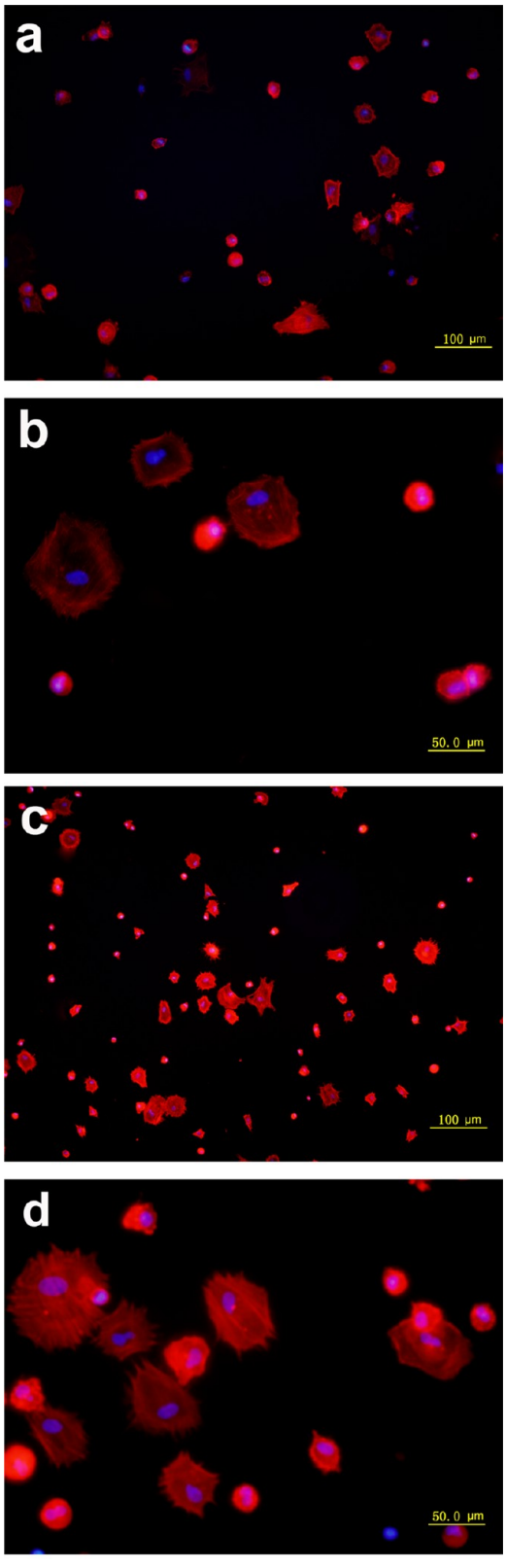

Figure 7. Fluorochromes micrography of rBMSCs cultured for 1 h shows that rBMSCs on an untreated tantalum surface (panels a and b) are rounded form and are less in number than those on the surfaces of the Ta_2O_5 nanotubes (panels c and d). Panels b and d are high-magnification photomicrographs of rBMSCs on the untreated tantalum surface and the surfaces of the Ta_2O_5 nanotubes, respectively.

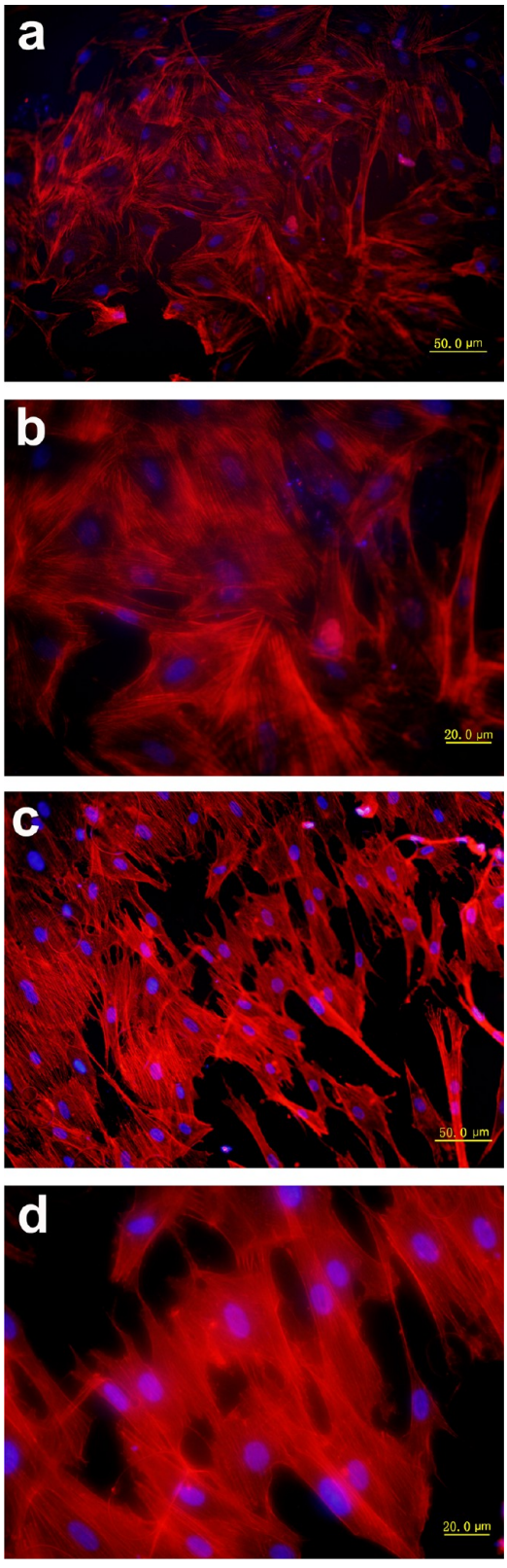

Figure 8. Fluorochromes micrography of rBMSCs after incubation for 48 h. rBMSCs on the nanotubes surface (panels c and d) have a more regular arrangement of the actin cytoskeleton, and more obviously have a polygonal and elongated form than on the untreated tantalum surface (panels a and b).

4. The results of the MTT assay show that there were significant differences between the untreated tantalum surface

and the surfaces of the Ta_2O_5 nanotubes during all incubation periods ($P < 0.01$). Both surface energy and high protein adsorption capacity being improved by Ta_2O_5 nanotube films are two important reasons. Some previous studies indicated that cells preferentially adhered well on hydrophilic surface with high surface energy and fibronectin adsorption, which is consistent with our results that there were more rBMSCs on the surfaces of the Ta_2O_5 nanotubes.[27,32−37] Besides improved hydrophilicity and surface energy, cells adhered to the 20-nm-thick surfaces of the Ta_2O_5 nanotubes easily, because a large number of protein nanoparticles had been absorbed on the nanotube films.[39] Moreover, previous study had demonstrated that the predicted size of surface occupancy by the head of an integrin heterodimer consisting of a $\hat{a}$-propeller of the R-chain and the A-domain of the $\hat{a}$-chain was ∼10 nm in diameter.[40] This suggests that the 20-nm diameters of the Ta_2O_5 nanotubes will allow clustering of integrins into the nearly closest packing possible, resulting in optimal integrin activation, which then enhanced the cell adhesion and proliferation on the surfaces of the nanotubes. On the other hand, the higher anticorrosion of the surfaces of the Ta_2O_5 nanotubes avoids abnormal apoptosis that is caused by released ions and corrosion products.

3.6. Osteogenesis-Related Genes Expression (Osterix, ALP, Collagen-I, and Osteocalcin) at the Untreated Tantalum Surface and the Surfaces of the Ta_2O_5 Nanotubes. In comparison with the untreated tantalum surface, the expression of Osterix (Osx), ALP, Collagen-I (Col-I), and Osteocalcin (OC) at the surfaces of the Ta_2O_5 nanotubes was significantly higher during all times, except for the significantly higher expression of Osx and OC on the untreated surface at day 14. (See Figure 5, $P < 0.01$.) Osteogenesis-related genes are strictly regulated to ensure the correct chronological order and that each gene has a unique expression profile.[11,18,19,21,−4146] In our study, gene expression also showed unique characteristics (see Figure 6). Osx is a zinc finger transcription factor specifically expressed by osteoblasts, which is important for osteoblast differentiation by directing preosteoblasts to immature osteoblasts.[42,43] In our study, the expression of Osx peaked and was much higher on the surfaces of the Ta_2O_5 nanotubes than on the untreated tantalum surface at an earlier times (day 3), suggesting that the surfaces of the Ta_2O_5 nanotubes have greater potential to induce rBMSCs differentiating into osteoblasts. In cell differentiation, the increase of ALP activity commits more cells to differentiate into the osteoblast lineage,[18,19,44] and Col-I is known to be an early osteogenitor marker and necessary to bone matrix formation.[40,43] In our study, ALP and Col-I expression was upregulated at earlier times (day 3) (see Figures 5 and 6), and Ta_2O_5 nanotubes surface had significantly higher expression levels of ALP and Col-I at all time points (Figure 5), suggesting that Ta_2O_5 nanotubes promote the rBMSCs differentiation, matrix formation, and mineralization on tantalum surface. Osteocalcin (OC) is secreted solely by osteoblasts. The OC expression correlates with the maturation of the osteoblast population and subsequent spontaneous mineralization.[46] The surfaces of the Ta_2O_5 nanotubes can stimulate the high expression level of OC in this study (see Figure 5), which means that Ta_2O_5 nanotubes can enhance rBMSCs matrix protein production and early osteogenesis.[45−47] All the gene expression results suggest that Ta_2O_5 nanotube array films stimulate the differentiation of BMSCs into osteoblasts and high expression of osteogenesis-related genes, and accelerate the osteogenesis response of tantalum.

It is particularly worth noting that the Osx and OC expression levels of rBMSCs on the untreated tantalum surface are higher than those on the surfaces of the Ta_2O_5 nanotubes at day 14 (see Figure 5d). These higher mRNA levels on the untreated tantalum surface probably attributed to a delayed osteogenic differentiation of rBMSCs cultured on the untreated tantalum surface, compared with the surfaces of the Ta_2O_5 nanotubes.[11]

3.7. Fluorescence Microscopy Image. After incubation for 1 and 2 h, the rBMSCs cultured on the untreated tantalum surface were rounded and less in number than those on the surfaces of the Ta_2O_5 nanotubes; moreover, the cells cultured on the surface of the nanotubes seem to have a polygonal morphology and spread more filopodia than those on the untreated tantalum surface (see Figure 7 and Figure S3 in the Supporting Information). After incubation for 24 and 48 h, compared to rBMSCs on the untreated tantalum surface, rBMSCs on the surface of the nanotubes seemed to show the more regular arrangement of an actin cytoskeleton, and, more obviously, a polygonal and elongated form (see Figures 8c and 8d, as well as Figures S4c and S4d in the Supporting Information). As is well-known, various types of physical stresses from the substrate morphology and topography can accelerate stem cells differentiation into a specific cell lineage.[20,22,39,44,45] In our study, it is most probable that this elongated morphology causes cellular cytoskeletal tension and stress of the rBMSCs cultured on the surface of the nanotubes, and then the cellular cytoskeletal tension and stress accelerate BMSCs differentiation into osteoblast cell lineage.[11,39,44]

4. CONCLUSIONS

Ta_2O_5 nanotube array films have been fabricated in the present study. After anodization, the nanotublar films significantly enhance the anticorrosion, hydrophilicity, and surface energy of pure tantalum, which resulted in a significant promotion in protein adsorption and the biological function of rabbit bone mesenchymal stem cells (rBMSCs).

Ta_2O_5 nanotube films can induce rBMSCs to differentiate into osteoblasts and activate the osteogenesis response, which suggest that Ta_2O_5 nanotube films can improve the biocompatibility of pure tantalum, and have a very good perspective of application in improving the osteoinductivity of tantalum.

■ ASSOCIATED CONTENT

Ⓢ Supporting Information

Bone mesenchymal stem cells (BMSCs) differentiate into osteoblasts and adipocytes; the crystal structures of pure tantalum, anodized tantalum, annealed Ta oxide nanotube film (XRD); fluorescence images of adherent rBMSCs at 2 h and 24 h. This material is available free of charge via the Internet at http://pubs.acs.org.

■ AUTHOR INFORMATION

Corresponding Author

*Tel.: +86 10 67391101 (H.Y.L., J.S.W.), +86 10 67099279 (Z.Z). Fax: +86 10 67391101 (H.Y.L., J.S.W.), +86 10 67099279 (Z.Z.). E-mail addresses: lhy06@bjut.edu.cn (H.Y.L.), wangjsh@bjut.edu.cn (J.S.W.), and zztttxl@hotmail.com or yuhuashi69@163.com (Z.Z.).

Notes

The authors declare no competing financial interest.

■ ACKNOWLEDGMENTS

This work is financially supported by National Natural Science Foundation of China (NSFC No. 51002004), Beijing Municipal Commission of Education Foundation (Nos. KZ201010005001 and KM201110005003), Guangxi Natural Science Foundation (No. 2010GXNSFB013009), State Key Laboratory of Electronic Thin Films and Integrated Devices (UESTC No. KFJJ201001), and City Board of Education Technology Innovation Platform (No. PXM2011_014226_07_000065).

■ REFERENCES

(1) Chaneliere, C.; Autran, J. L.; Devine, R. A. B.; Balland, B. *Mater. Sci. Eng.: R.* **1998**, *22*, 269−322.
(2) Bermúdez, M. D.; Francisco, J.; Carrión, F. J.; Nicolás, G. M.; López, R. *Wear* **2005**, *258*, 693−700.
(3) Zitter, H.; Plenk, H. *J. Biomed. Mater. Res.* **1987**, *21*, 881−896.
(4) Meneghini, R. M.; Ford, K. S.; McCollough, C. H.; Hanssen, A. D.; Lewallen, D. *J. Arthroplasty* **2010**, *25*, 741−747.
(5) Fernández-Fairen, M.; Sala, P.; Dufoo, M., Jr.; Ballester, J.; Murcia, A.; Merzthal, L. *Spine* **2008**, *33*, 465−472.
(6) Kamath, A. F.; Lee, G.; Sheth, N. P.; Nelson, C. L.; Garino, J. P.; Israelite, C. L. *J. Arthroplasty* **2011**, *26*, 1390−1395.
(7) Balla, V. K.; Banerjee, S.; Bose, S.; Bandyopadhyay, A. *Acta Biomater.* **2010**, *6*, 2329−2334.
(8) Roy, M.; Balla, V. K.; Bandyopadhyay, A.; Bose, S. *ACS Appl. Mater. Interfaces* **2012**, *4*, 577−580.
(9) Macionczyk, F.; Gerold, B.; Thull, R. *Surf. Coat. Technol.* **2001**, *142−144*, 1084−1087.
(10) Sevilla, P.; Aparicio, C.; Planell, J. A.; Gil, F. *J. Alloys Compd.* **2007**, *439*, 67−73.
(11) Stiehler, M.; Lind, M.; Mygind, T.; Baatrup, A.; Dolatshahi-Pirouz, A.; Li, H.; Foss, M.; Besenbacher, F.; Kassem, M.; Bünger, C. *J. Biomed. Mater. Res., Part A* **2008**, *86A*, 448−458.
(12) Li, H. Y.; Wang, J. S.; Huang, K. L.; Sun, G. S.; Zhou, M. L. *Mater. Lett.* **2011**, *65*, 1180−1190.
(13) Huo, K. F.; Wang, H. R.; Zhang, X. M.; Cao, Y.; Chu, P. K. *Chempluschem* **2012**, *77*, 323−329.
(14) Zhao, J.; Xu, R.; Wang, X; Li, Y. *Corros. Sci.* **2008**, *50*, 1593−1597.
(15) de Arruda Rodrigues, C.; de Tacconi, N. R.; Chanmanee, W.; Rajeshwar, K. *Electrochem. Solid-State Lett.* **2010**, *13*, B69−B72.
(16) Allam, N. K.; Feng, X. J.; Grimes, C. A. *Chem. Mater.* **2008**, *20*, 6477−6481.
(17) El-Sayed, H. A.; Birss, V. I. *Nano Lett.* **2009**, *9*, 1350−1355.
(18) Zhao, L.; Hu, L.; Huo, K. F.; Zhang, Y.; Wu, Z.; Chu, P. K. *Biomaterials* **2010**, *31*, 8341−8349.
(19) Yu, W.; Jiang, X.; Zhang, F.; Xu, L. *J. Biomed. Mater. Res. A* **2010**, *94A*, 1012−1022.
(20) Shekaran, A.; Garcia, A. J. *BBA−Gen. Subj.* **2011**, *1810*, 350−360.
(21) Bjursten, L. M.; Rasmusson, L.; Oh, S.; Smith, G. C.; Karla, S.; Brammer, K. S.; Jin, S. *J. Biomed. Mater. Res., Part A* **2010**, *92A*, 1218−1224.
(22) Wang, N.; Li, H. Y.; Lv, W. L.; Li, J. H.; Wang, J. S.; Zhang, Z. T.; Liu, Y. R. *Biomaterials* **2011**, *32*, 6900−6911.
(23) Ruckh, T.; Porter, J. R.; Allam, N. K.; Feng, X.; Grimes, C. A.; Popat, K. C. *Nanotechnology* **2009**, *20*, 045102.
(24) Van Oss, C. J.; Giese, R. F.; Good, R. J. *Langmuir* **1990**, *6*, 1711−1713.
(25) Park, H.; Temenoff, J. S.; Tabata, Y.; Caplan, A. I.; Mikos, A. G. *Biomaterials* **2007**, *28*, 3217−3227.
(26) Kuo, Y. *J. Electrochem. Soc.* **1992**, *139*, 579−583.
(27) Sakai, Y.; Ninomiya, S; Hiraoka, K. *Surf. Interface Anal.* **2011**, *43*, 1605−1609.
(28) Das, K.; Bose, S.; Bandyopadhyay, A. *J. Biomed. Mater. Res., Part A* **2009**, *90A*, 225−237.
(29) Michiardi, A.; Aparicio, C.; Ratner, B. D.; Planell, J. A.; Gil, J. *Biomaterials* **2007**, *28*, 586−594.
(30) Arima, Y.; Iwata, H. *Biomaterials* **2007**, *28*, 3074−3082.
(31) Das, K.; Bose, S.; Bandyopadhyay, A. *Acta Biomater.* **2007**, *3*, 573−585.
(32) Wilson, C. J.; Clegg, R. E.; Leavesley, D. I.; Pearcy, M. J. *Tissue Eng.* **2005**, *11*, 1−18.
(33) Hovgaard, M. B.; Rechendorff, K.; Chevallier, J.; Foss, M.; Besenbacher, F. *J. Phys. Chem. B* **2008**, *112*, 8241−8249.
(34) Tsai, J. A.; Lagumdzija, A.; Stark, A.; Kindmark, H. *Cell Biochem. Funct.* **2007**, *25*, 245−249.
(35) Green, R. J.; Davies, M. C.; Roberts, C. J.; Tendler, S. J. B. *Biomaterials* **1999**, *20*, 385−391.
(36) Valenick, L. V.; Hsia, H. C.; Schwarzbauer, J. E. *Exp. Cell Res.* **2005**, *309*, 48−55.
(37) Veevers-Lowe, J.; Ball, S. G.; Shuttleworth, A.; Kielty, C. M. *J. Cell Sci.* **2011**, *124*, 1288−1300.
(38) MacDonald, D. E.; Deo, N.; Markovic, B.; Stranick, M.; Somasundaran, P. *Biomaterials* **2002**, *23*, 1269−1279.
(39) Oh, S.; Brammer, K. S.; Li, Y. S. J.; Teng, D.; Engler, A. J.; Chien, S.; Jin, S. *Proc. Natl. Acad. Sci. U.S.A.* **2009**, *106*, 2130−2135.
(40) Takagi, J.; Petre, B. M.; Walz, T.; Springer, T. A. *Cell* **2002**, *110*, 599−611.
(41) Franceschi, R. T.; Ge, C.; Xiao, G.; Roca, H.; Jiang, D. *Cells Tissues Organs* **2007**, *189*, 196−207.
(42) Nakashima, K.; Zhou, X.; Kunkel, G.; Zhang, Z.; Deng, J. M.; Behringer, R. R.; de Crombrugghe, B. *Cell* **2002**, *108*, 17−29.
(43) Zhang, C. *J. Orthop. Surg. Res.* **2010**, *5*, 37−43.
(44) Olivares-Navarrete, R.; Hyzy, S. L.; Hutton, D. L.; Erdman, C. P.; Wieland, M.; Boyan, B. D.; Schwartz, Z. *Biomaterials* **2010**, *31*, 2728−2735.
(45) Khan, M. R.; Donos, N.; Salih, V.; Brett, P. M. *Bone* **2012**, *50*, 1−8.
(46) Desbois, C.; Karsenty, G. *J. Cell. Biochem.* **1995**, *57*, 379−383.
(47) Schlegel, K. A.; Thorwarth, M.; Plesinac, A.; Wiltfang, J.; Rupprecht, S. *Clin. Oral Implants Res.* **2006**, *17*, 666−672.